Single-Feed Multi-Beam Conformal Transmitarrays with Phase and Amplitude Modulations

Li-Zhao Song, *Student Member, IEEE,* Xuan Wang, and Pei-Yuan Qin, *Senior Member, IEEE*

Abstract— Single-feed multi-beam conformal transmitarrays using a superposition method are presented in this paper. The arrays consist of ultra-thin Huygens elements with independent amplitude and phase manipulations. Three cylindrical conformal transmitarrays with dual-beam radiation patterns are designed at 10 GHz, producing dual beams at ±30º, +30º and -20º, +30º and -10º, respectively. As an experimental validation, the prototype with symmetrical dual beams is fabricated and measured. Two beams at +29° and -28° along H-plane are achieved with a measured 18.29 dBi peak gain. The gain difference between the two beams is 0.13 dB. Good agreement between simulation and measurement is observed.

Index Terms— Conformal antennas, multi-beam, transmitarray.

I. INTRODUCTION

Multi-beam antennas are widely hailed as a key technology for the current fifth generation (5G) and beyond 5G (B5G) wireless communications networks. They play a crucial role to serve point-to-multi-point and multi-point-to-multi-point links, thus leading to efficient and high-capacity communications [1]-[3]. More specifically, for applications such as broadcasting and data distribution, single-feed multi-beam antennas can serve multiple users at the same time to achieve point-to-multi-point communications. Within this scope, substantial efforts have been devoted to multi-beam reflectarrays [4]-[5] and transmitarrays [6]-[7] due to their advantages of flexible beam synthesis and high gains without complicated and lossy feed networks. Compared to reflectarrays, transmitarrays do not have the problem of feed blockages [8]-[12].

On the other hand, conformal antennas are highly desirable for airborne platforms with curved shapes, e.g., UAVs and aircrafts, to meet the aerodynamic requirements [13]-[16]. Since the fuselage of the airborne platforms can serve as the transmitting aperture with the feed located inside the aircrafts, conformal transmitarrays are particularly suitable for this application as part of the platform surface can accommodate the transmitting aperture with the feed placed behind. It is proven that one of the most cost-effective and practical ways for conformal transmitarray implementations is to utilize up-to-0.5-mm-thick elements, making transmitting apertures easily bent into curved shapes [17]. Such a stringent constraint on the thickness of array elements imposes more difficulties in
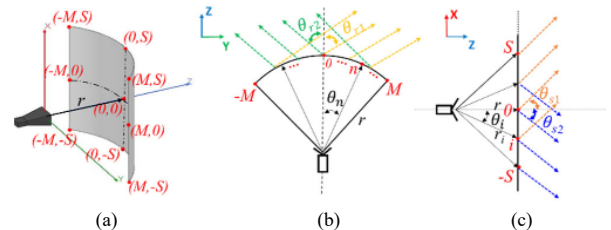

Fig. 1. A cylindrical conformal transmitarray. (a) 3-D view. (b) Along yoz plane (H-plane). (b) Along xoz plane (E-plane).

designing single-feed multi-beam conformal transmitarrays.

To date, optimization algorithms [6]-[7] with phase manipulations are usually employed to develop single-feed dual-/multi-beam planar transmitarrays. In [6], a particle swarm optimization (PSO) method is applied along with a phase-variable four-metal-layer element to obtain a dual-beam radiation pattern at ±25°. In [7], a modified intersection approach is employed to synthesize a quad-beam pattern of a low-profile transmitarray antenna with quad-layer 3-dipole elements. Four symmetrical beams are realized at θ=25°, and φ=0°, 90°, 180° and 270°, respectively. In [18], with a triple-layer meta-atom-based element proposed for phase compensations, an alternating projection method (APM) is utilized to synthesize a dual-beam transmitarray at ±30°.

It is noticeable that the above-mentioned multi-beam designs are all for planar transmitarrays. Very few works have been published for conformal ones. Besides, most of the reported single-feed multi-beam designs resort to phase-only optimization algorithms. It should be noted that this method does not always guarantee a satisfactory result due to the possibility of non-convergence of the algorithm, especially for conformal arrays with complicated aperture configurations. On the other hand, a superposition method, using element phase and amplitude manipulations, is much simpler and can promise a stable solution. However, it is very challenging to develop both phase and amplitude controllable transmissive elements with a small thickness for conformal designs. In [5], multi-beam reflectarrays using the superposition method are presented. A C-shaped reflective element is proposed with independent phase and amplitude manipulations. The reflectarrays can generate multiple beams with arbitrary radiation angles based on the amplitude and phase modulations along the apertures. Unfortunately, to date, there are very few works reported on

conformal multi-beam transmitarrays using the superposition method.

In this paper, single-feed multi-beam conformal transmitarrays are developed using the superposition method. To enable the implementations of conformal prototypes, an ultra-thin element with both phase and amplitude controls is developed based on the Huygens element in [17]. It should be noted that the Huygens model in [17] can achieve a phase modulation only. In order to extend its capability to provide amplitude control, new theoretical analysis and simulations are required. To validate the proposed methods, three cylindrical transmitarrays have been designed with symmetric/asymmetric dual beams along H-plane at 10 GHz. Finally, a prototype is fabricated and measured. To the authors' best knowledge, this work represents the first reported research in single-feed multi-beam conformal transmitarrays.

II. MULTI-BEAM CONFORMAL TRANSMITARRAY WITH SUPERPOSITION METHOD

Fig. 1 (a) shows the sketch of a cylindrical conformal transmitarray. It is composed of $2M+1$ and $2S+1$ elements along yoz (H-) and xoz (E-) planes, respectively. Dual beams can be synthesized along these two planes independently. The design principle is explained as follows.

If only considering the 1-D circular array along yoz plane fed by a source located at the centre, as shown in Fig. 1 (b), its array factor can be calculated from (1). On the other hand, for the linear array along xoz plane fed by the same source as in Fig. 1 (c), its array factor will follow (2).

$$f_1(\theta) = \sum_{n=-M}^{M} f_h(\theta_n)\exp(j(kr(\cos(\theta-\theta_n)-\cos(\theta))+\varphi_{cn})),$$
(1)

$$f_2(\theta) = \sum_{i=-S}^{S} f_h(\theta_i)\exp(j(k(r-r_i+x_i\sin(\theta))+\varphi_{sn})),$$
(2)

where $f_h(\theta)$ represents the radiation pattern of the feed source, k is the propagation constant in free space, r denotes the radius of the cylindrical array, r_i is the focal length of the i-th element along xoz plane, θ_n and θ_i represents the offset angle at the n-th element and i-th element along yoz and xoz planes, respectively, x_i represents the position of the i-th element with respect to the center point along x-axis, φ_{cn} and φ_{sn} are the compensation phase values along yoz and xoz planes, respectively. We assume that the element pattern is a uniform one as from an ideal point source. Therefore, the far-field radiation patterns of these two 1-D arrays can be represented by (1)-(2).

If considering a uniform illumination from the feed source in Fig. 1 (b), to radiate a single beam at θ_{r1}, the desired compensation phase at the n-th element can be obtained as (3). The compensation amplitude is constantly 1. Therefore, the complex compensation factor I_{n1} is expressed in (4). For a single beam at θ_{r2}, the factor I_{n2} can be obtained from (5).

$$\varphi_{cn1} = kr[\cos\theta_{r1} - \cos(\theta_{r1}-\theta_n)]$$
(3)

$$I_{n1} = \exp(jkr(\cos\theta_{r1} - \cos(\theta_{r1}-\theta_n)))$$
(4)

$$I_{n2} = \exp(jkr(\cos\theta_{r2} - \cos(\theta_{r2}-\theta_n)))$$
(5)

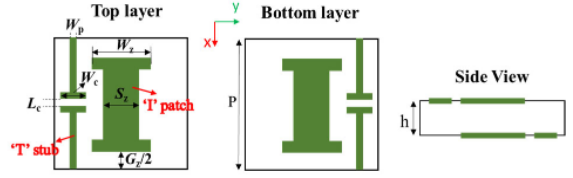Fig. 2. Dual-layer Huygens element structure (h=0.508 mm).

Applying the superposition method, dual beams at θ_{r1} and θ_{r2} can be achieved simultaneously from the vector addition of (4) and (5). Consequently, the complex compensation factor I_n for a dual-beam radiation along yoz plane should satisfy (6), which requires both phase and amplitude modulations.

$$I_n = I_{n1} + I_{n2} = \exp(jkr(\cos\theta_{r1} - \cos(\theta_{r1}-\theta_n))) + \exp(jkr(\cos\theta_{r2} - \cos(\theta_{r2}-\theta_n))) = |I_n|\exp(j\varphi_n),$$
(6)

where $|I_n|$ and φ_n denote the amplitude and phase compensation values at the n-th element, respectively.

Besides, if two beams are desired along xoz plane at θ_{s1} and θ_{s2}, as sketched in Fig. 1 (c). the complex compensation factor I_i along this plane should satisfy (7) based on the superposition method.

$$I_i = \exp(jk(r_i - r - x_i\sin\theta_{s1})) + \exp(jk(r_i - r - x_i\sin\theta_{s2})) = |I_i|\exp(j\varphi_i),$$
(7)

where $|I_i|$ and φ_i denote the amplitude and phase compensation values at the i-th element, respectively.

Subsequently, for the compensation factors along a 2-D cylindrical transmitting surface in Fig. 1 (a), the compensation factors of elements along the middle circular cross section are considered first by following (6). Then these elements will serve as the base to calculate the compensation factors of other elements in each column along x-axis by following (7). Finally, one can obtain the final compensation factor I_{ni} at a random point along the conformal transmitting surface as (8). In practice, there is an illumination taper from the feed source, therefore the desired transmission coefficient is modified as (9).

$$I_{ni} = I_n * I_i = |I_n||I_i|\exp(j(\varphi_i + \varphi_n))$$
(8)

$$T_{ni} = \frac{|I_n||I_i|}{f_h(\theta_n)f_h(\theta_i)}\exp(j(\varphi_i + \varphi_n))$$
(9)

A. Element Design

As discussed in Section I, the major challenge of the superposition method is to achieve both phase and amplitude manipulations. Moreover, to maintain the easy implementations of conformal transmitarrays, the element should have an ultra-thin profile. In light of these concerns, the dual-layer Huygens element proposed in [17] is further extended to allow both phase and amplitude controls. As illustrated in Fig. 2, the element consists of two metal layers printed on a 0.508-mm-thick substrate (dielectric constant ε_r=3.55, tan δ=0.0027). The element periodicity P is 8.5 mm. Two symmetric "I" shape patches on the top and bottom layers are designed to produce a magnetic response, while two pairs of head-to-head "T" stubs are printed diagonally on the margins of two sides to support electric responses. The electric and magnetic surface impedances can be independently tuned by adjusting the dimensions of "T" stubs and "I" patches, respectively.

As discussed in [19], to enable both amplitude and phase modulations of Huygens metasurfaces, the corresponding surface impedances for an arbitrary transmission coefficient of $|T_n|e^{j\varphi_n}$ are generalized as (10)-(12).

$$Z_e = j\eta/(2\tan((\varphi_n \pm \alpha)/2)), \qquad (10)$$

$$Z_m = -j2\eta\tan((\varphi_n \mp \alpha)/2), \qquad (11)$$

$$\alpha = arctan(\sqrt{1-|T_n|^2}/|T_n|), \qquad (12)$$

where η denotes the wave impedance in free space, Z_e and Z_m are the surface electric and magnetic impedances, respectively. To simplify the expressions of equations, α is defined and related to the transmission amplitude. It will be substituted into (10)-(11).

In this work, a set of Huygens elements, i.e., totally 32 elements, for 2-bit-amplitude and 3-bit-phase modulations are developed. It is found that the directivity reduction of a cylindrical transmitarray would be around 0.2 dB for a 3-bit digital phase discretization and a 2-bit digital amplitude discretization, compared to the continuous phase and amplitude modulations. For each specific transmitting phase and amplitude, the corresponding surface impedances can be calculated from (10)-(11). Each pair of surface impedances corresponds to a specific element configuration for desired transmission amplitude and phase. The element is simulated in 3-D simulation software ANSYS HFSS. Two pairs of master-slave boundaries are defined along x- and y- axes, and two Floquet ports are assigned along z-axis. To demonstrate the element performance, the transmission coefficients of 2-bit amplitude-modulated elements with a constant transmission phase value of -60° are shown in Fig. 3. Their properties are summarized in Table I. Other physical parameters are unchanged as P=8.5 mm, S_z=2.3 mm, G_z=1.7 mm, and W_p=0.2 mm. Besides, Fig. 4 shows the transmission coefficients of 3-bit phase-modulated elements with a fixed amplitude value of 0.5. The properties of them are given in Table II. Similar results are obtained for other amplitude and phase values. They are not listed here for brevity. It is noticed that the developed elements have a narrow bandwidth as the ones in [17]. This is due to the inherent narrow-band property of the Huygens element, as it is difficult to keep the surface impedance constant in a wide frequency band. Using multi-layer Huygens elements or multi-layer polarization conversion surfaces [20] could potentially increase the bandwidth.

B. Conformal Transmitarray Design

To validate the design theory, a dual-beam conformal transmitarray is developed with a cylindrical shape. The desired two beams are defined as $\theta_{r1, r2}$=±30° along yoz plane. For simplicity, along xoz plane, both beams will point to boresight. The conformal array has a radius of r=165.8 mm. It consists of 32×33=1056 elements with a cross-sectional area of 243 mm×281 mm projected on xoy plane. A standard gain horn LB-75-10 from A-INFO is placed at the centre point of the transmitarray for a -10-dB edge illumination. The realized gain of the feed horn from datasheet is 10.15 dBi at 10 GHz, and its normalized radiation pattern is represented as $f_h(\theta)$ in (13), by
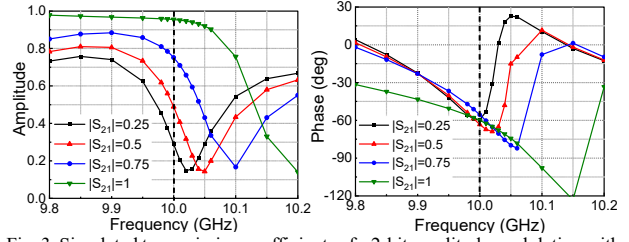

Fig. 3. Simulated transmission coefficients of a 2-bit amplitude modulation with a -60° phase value at 10 GHz. (a) Amplitude. (b) Phase.
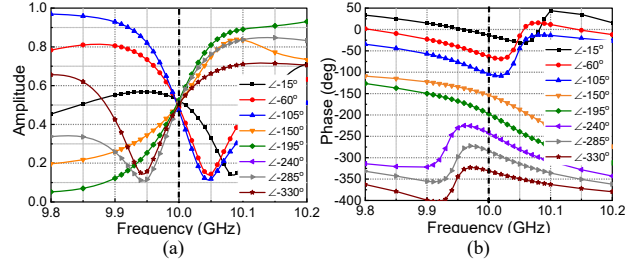

Fig. 4. Simulated transmission coefficients of a 3-bit phase modulation with a fixed transmission amplitude of 0.5 at 10 GHz. (a) Amplitude. (b) Phase.

TABLE I
2-BIT AMPLITUDE-MODULATED HUYGENS ELEMENTS WITH A PHASE OF -60°

Element No.	$|S_{21}|$	$\angle S_{21}$	Wz /mm	Wc /mm	Lc /mm
1	0.95	-60°	4.05	1.45	0.1
2	0.73	-57°	4.13	1.3	0.15
3	0.49	-61°	4.17	1.25	0.15
4	0.29	-60°	4.19	1.22	0.15

TABLE II
3-BIT PHASE-MODULATED HUYGENS ELEMENTS WITH AN AMPLITUDE OF 0.5

Element No.	$|S_{21}|$	$\angle S_{21}$	Wz /mm	Wc /mm	Lc /mm
1	0.51	-14°	4.1	1.32	0.22
2	0.49	-61°	4.17	1.25	0.15
3	0.46	-104°	4.2	1.3	0.1
4	0.52	-155°	4.13	1.35	0.4
5	0.52	-197°	4.17	1.29	0.3
6	0.47	-242°	4.2	1.26	0.24
7	0.5	-284°	4.23	1.24	0.2
8	0.49	-331°	4.27	1.38	0.2

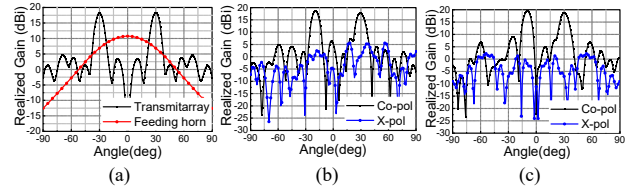Fig. 5. Dual-beam radiation patterns. (a) At ±30°. (b) At 30° and -20°. (c) At 30° and -10°.

considering the 3-dB beamwidth from its datasheet.

$$f_h(\theta) = cos^{3.5}(\theta) \qquad (13)$$

Based on (9), the desired complex transmission coefficients can be calculated as (14). Considering that the realizable transmission amplitude varies between 0-1, the magnitude of T_{ni} is normalized.

$$T_{ni} = normalize\left(\frac{\cos\left(\frac{krsin(\theta_n)}{2}\right)}{cos^{3.5}(\theta_n)cos^{3.5}(\theta_i)}\right)\exp(jk\big(r_i - r +$$

$$\sqrt{3}r(1 - \cos(\theta_n))/2\big)) \qquad (14)$$

Once the transmission coefficient is calculated for a specific position on the cylindrical surface, we can retrieve it from the 32 developed Huygens elements in terms of the transmission amplitude and phase. Finally, the configuration of the 3-D cylindrical conformal transmitarray would be determined. The simulated radiation patterns of the transmitarray and the feeding horn are plotted in Fig. 5 (a). The peak gain of the horn is 10.7 dBi. For the conformal transmitarray, dual beams at the desired directions of ±30° have been achieved with a peak realized gain of 18.3 dBi. It should be noted that the radiation performance will be improved if oblique incidences of each element on the transmitting aperture are considered. However, this will make the design time-consuming.

As a generalized verification, two more conformal transmitarrays with asymmetric dual beams along yoz plane are designed. They have the same physical parameters and feed sources as the symmetric one. One of them is designed to radiate beams at 30° and -20°, while the other one radiates dual beams at 30° and -10°. The simulated radiation patterns are shown in Fig. 5 (b) and (c). The peak gain values are 18.7 dBi and 19.6 dBi for the two transmitarrays, respectively. The gain differences between the two beams are around 1 dB. The sidelobe levels from both designs are less than -10 dB with respect to the peak values. Cross-polarization levels are lower than -13 dB and -17 dB for the two prototypes, respectively.

III. Prototype Fabrication And Measurement

As an experimental validation, the cylindrical transmitarray prototype with dual beams at ±30° is fabricated and measured. The unfolded transmitting surface has two metal layers printed on one dielectric substrate with a thickness of 0.508 mm. Firstly, standard printing circuit board (PCB) technology is utilized to fabricate the unfolded planar transmitting surface on a low-cost Taconic substrate (dielectric constant εr=3.5±0.1, tan δ=0.0018) [21]. It should be noted that polytetrafluoroethylene (PTFE)-based substrate material should be chosen in order to realize an easy bending. Meanwhile, 3-D printing technology is applied to print a cylindrical hollow frame. Secondly, the transmitting surface is bent and attached onto this frame for a fixed cylindrical configuration. Photographs of the fabricated prototype and measurement setup are provided in Fig. 6.

The simulated and measured |S₁₁| are compared in Fig. 7 (a). Both of them are lower than -10 dB from 9.6-10.5 GHz. Far-field radiation patterns are measured in a Microwave Vision Group (MVG) compact range located at University of Technology Sydney, Australia. The simulated and measured peak gain values versus frequency are shown in Fig. 7 (a). It is noticed that the optimal working frequency appears at 10 GHz from simulation with a peak gain of 18.3 dBi. During the measurement, the operating frequency shifts to 10.1 GHz with a peak gain of 18.29 dBi. The measured aperture efficiency is 16.2%. The aperture efficiency is calculated as the ratio of the antenna realized gain and the maximal directivity calculated from the array aperture. A frequency shift of around 2% appears
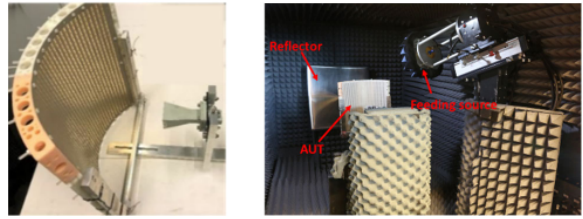

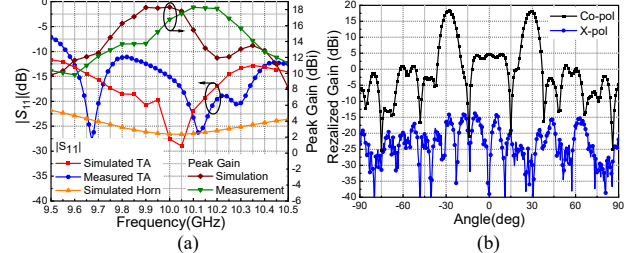Fig. 6. Photographs of antenna measurement.

Fig. 7. (a) Simulation and measurement results of input reflection coefficients and peak gains versus frequency. (b) Measured radiation pattern at 10.1 GHz.

during the measurement. It can be mostly attributed to the following factors. First, it can be due to the inaccuracies of the 3-D printed cylindrical frame. The curvature of the printed frame may deviate from the simulated models. Second, it can be due to the deviations of the dielectric constant of the substrate. Third, it can be because of the alignment errors between the transmitting surface and feeding source. A 3-dB gain bandwidth of 3.5% is realized from 9.95 GHz to 10.3 GHz. The measured radiation pattern at the optimal frequency of 10.1 GHz is shown in Fig. 7 (b). The measured dual beams are at +29° and -28° with a 0.13-dB gain difference. The sidelobe levels are below -13.6 dB. The measured cross-polarization levels are lower than -30 dB along H-plane. Besides, the radiation patterns remain stable across the frequency band from 10 GHz to 10.3 GHz. They are not shown here due to the limited space.

The previously reported single-feed multi-beam transmitarrays [6]-[7], [18] have planar configurations with multiple metal layers and large aperture thickness. Besides, only phase modulations of their elements are considered. This work represents the first research in single-feed multi-beam conformal transmitarrays with both phase and amplitude modulations.

IV. Conclusion

Single-feed multi-beam conformal transmitarrays are presented based on the superposition method. Independent control of both transmission amplitude and phase is realized based on Huygens metasurface, enabling 2-bit-amplitude and 3-bit-phase modulations. Several cylindrical transmitarrays are constructed with different radiation patterns to validate the design principle. A dual-beam prototype is fabricated and measured, yielding two beams at +29° and -28° along H-plane with a peak gain of 18.29 dBi at 10.1 GHz. The synthesis method can also be extended for circularly or dual-linearly polarized transmitarrays by using appropriate array elements. The proposed conformal transmitarrays are expected to be applied to point-to-multi-point wireless communications to improve channel efficiency and capacity.

REFERENCES

[1] W. Hong et al. "Multibeam antenna technologies for 5G wireless communications," *IEEE Trans. Antennas Propag.,* vol. 65, no. 12, pp. 6231–6249, Dec. 2017.

[2] Y. J. Guo and R. W. Ziolkowski, "Advanced antenna array engineering for 6G and beyond wireless communications," *IEEE Press/Wiley,* Oct. 2021.

[3] Y. J. Guo, M. Ansari, R. W. Zilkowski and N. J. G. Fonseca, "Quasi-optical multi-beam antenna technologies for B5G and 6G mmwave and THz networks: a review," *IEEE Open Journal of Antennas and Propagation,* DOI: 10.1109/OJAP.2021.3093622.

[4] P. Nayeri, F. Yang, A. Z. Elsherbeni, "Design and experiment of a single-feed quad-beam reflectarray antenna," *IEEE Trans. Antennas Propag.,* vol. 60, no. 2, pp. 1166-1171, Feb. 2012.

[5] L. Bao, R. Y. Wu, X. Fu, Q. Ma, G. D. Bai, J. Mu, R. Jiang, T. J. Cui, "Multi-beam forming and controls by metasurface with phase and amplitude modulations," *IEEE Trans. Antennas Propag.,* vol. 67, no. 10, pp. 6680-6685, Oct. 2019.

[6] A. H. Abdelrahman, P. Nayeri, A. Z. Elsherbeni, F. Yang, "Single-feed quad-beam transmitarray antenna design," *IEEE Trans. Antennas Propag.,* vol. 64, no. 3, pp. 953-959, Mar. 2016.

[7] A. Aziz, F. Yang, S. Xu, M. Li, "A low-profile quad-beam transmitarray," *IEEE Antennas Wireless Propag. Lett.*, vol. 19, no. 8, pp. 1340-1344, Aug. 2020.

[8] S. Gaber, S. H. Zainud-Deen, and H. A. E. Malhat, *Analysis and Design of Reflectarrays/Transmitarrays Antennas*. Sunnyvale, CA, USA: LAP LAMBERT Academic Publ, 2014.

[9] F. Wu, R. Lu, J. Wang, Z. H. Jiang, W. Hong and K. -M. Luk, "Circularly-polarized one-bit reconfigurable ME-dipole reflectarray at X-band," *IEEE Antennas Wireless Propag. Lett.*, early access, Dec. 2021.

[10] P.-Y. Feng, S.-W. Qu, S. Yang, L. Shen and J. Zhao, "Ku-band transmitarrays with improved feed mechanism," *IEEE Trans. Antennas Propag.,* vol. 66, no. 6, pp. 2883-2891, Jun. 2018.

[11] X. Yi, T. Su, X. Li, B. Wu and L. Yang, "A double-layer wideband transmitarray antenna using two degrees of freedom elements around 20 GHz," *IEEE Trans. Antennas Propag.,* vol. 67, no. 4, pp. 2798-2802, Apr. 2019.

[12] F. Wu, J. Wang, R. Lu, X. Xia, W. Hong and K.-M. Luk, "Wideband and low cross-polarization transmitarray using 1 bit magnetoelectric dipole elements," *IEEE Trans. Antennas Propag.,* vol. 69, no. 5, pp. 2605-2614, May 2021.

[13] J.-J. Peng, S.-W. Qu, M. Xia, and S. Yang, "Conformal phased array antenna for unmanned aerial vehicle with ±70° scanning range," *IEEE Trans. Antennas Propag.,* vol. 69, no. 8, pp. 4580-4587, Aug. 2021.

[14] S. Xiao, *et al.*, "Practical implementation of wideband and wide-scanning cylindrically conformal phased array," *IEEE Trans. Antennas Propag.,* vol. 67, no. 8, pp. 5729-5733, Aug. 2019.

[15] P.-Y. Qin, L.-Z. Song, Y. J. Guo, "Beam steering conformal transmitarray employing ultra-thin triple-layer slot elements," *IEEE Trans. Antennas Propag.,* vol. 67, no. 8, pp. 5390-5398, Aug. 2019.

[16] M. Beccaria, P. Pirinoli, F. Yang, "Preliminary results on conformal transmitarray antennas", *IEEE International Symposium on Antennas and Propagation & USNC/URSI National Radio Science Meeting*, 2018.

[17] L.-Z. Song, P.-Y. Qin, and Y. J. Guo, "A high-efficiency conformal transmitarray antenna employing dual-layer ultra-thin Huygens element," *IEEE Trans. Antennas Propag.,* vol. 69, no. 2, pp. 848-858, Feb. 2021.

[18] H.-X. Xu, T. Cai, Y.-Q. Zhuang, Q. Peng, G.-M. Wang, J.-G. Liang, "Dual-mode transmissive metasurface and its applications in multibeam transmitarray," *IEEE Trans. Antennas Propag.,* vol. 65, no. 4, pp. 1797-1806, Apr. 2017.

[19] B. O. Zhu, K. Chen, N. Jia, L. Sun, J. Zhao, T. Jiang, and Y. Feng, "Dynamic control of electromagnetic wave propagation with the equivalent principle inspired tunable metasurface," *Scientific reports*, vol. 4, no. 1, pp. 1-7, May 2014.

[20] H.-P. Li, G.-M. Wang, T. Cai, H. Hou, W. Guo, "Wideband transparent beam-forming metadevice with amplitude-and phase-controlled metasurface," *Phys. Rev. Applied,* vol. 11, no. 1, Jan. 2019.

[21] https://www.agc-multimaterial.com/page/rf-35-71.html